at 25 °C.[14] In this work, we attempted to analyze the complicated oxidation mechanism of the oxygenated compound **3** in water-saturated methylene chloride. During the autoxidation process, several resonances of oxygen-17 enriched species were detected at low frequencies (Figure 3). The resonance absorption at δ = 11.1 ppm ($\Delta\nu_{1/2}$ = 2080 Hz) is characteristic of $H_2{}^{17}O$, and two sharp resonances at δ = 168.5 and 174.3 ppm can be assigned to $H_2{}^{17}O_2$. The two latter peaks must correspond to hydrogen peroxide in two different environments. Only the resonance at 174.3 ppm is observed for $H_2{}^{17}O_2$ dissolved in dry toluene. The second peak at 168.5 ppm is then probably due to $H_2{}^{17}O_2$ in microscopic water droplets in suspension, which are always present in organic solutions when a two-phased preparative system is used.

From the presence of enriched water and hydrogen peroxide formed during the oxidation process, the following reaction scheme may be proposed:

$$PFe^{II} + {}^*O_2 \rightleftharpoons PFe^{II}\text{–}{}^*O_2$$

$$PFe^{II}\text{–}{}^*O_2 + H_2O \rightarrow [PFe^{III}\cdots{}^*O_2{}^{\bullet-}\cdots HOH]$$

$$[PFe^{III}\cdots{}^*O_2{}^{\bullet-}\cdots HOH] \rightarrow PFe^{III}\text{–}OH^- + H{}^*O_2{}^\bullet$$

$$2H{}^*O_2{}^\bullet \rightarrow H_2{}^*O_2 + {}^*O_2$$

$$H_2{}^*O_2 \rightarrow H_2{}^*O + \tfrac{1}{2}{}^*O_2$$

This scheme seems to be in agreement with the autoxidation of hemoproteins.[48,49] Indeed, the replacement of histidine E7 in the α-chains of HbA by a potentially more strongly H-bonding residue, tyrosine (as in HbM Boston), leads to easier autoxidation probably due to H bonding to molecular oxygen strong enough to liberate a superoxide anion.[50] In the model compounds, it seems reasonable that water allows the proton-driven oxidation to form a labeled hydrosuperoxide radical that gives $H_2{}^*O_2$ and $H_2{}^*O$ in further reactions.

The NMR spectrum in methylene chloride also exhibits a sharp resonance at 372.9 ppm ($\Delta\nu_{1/2}$ = 108 Hz) that has not yet been assigned confidently. It could be due to an oxidation reaction of the solvent molecules since no such resonance is observed when toluene is used as a solvent.

^{17}O NMR appears therefore of great potential value for the analysis of both the nature and the reactivity of the Fe–O_2 moiety in hemoprotein models.

Acknowledgment. Financial support from EEC (Contract No. ST2*439), NATO (Collaborative Research Grant No. 0536/88), the Research Committee of the University of Ioannina (Greece), the Institut National de la Santé et de la Recherche Médicale (France), and EMBO (short-term fellowship to I.P.G.) is gratefully acknowledged. We appreciated useful comments and suggestions from Dr. J. M. Lhoste and the referees.

(48) Weiss, J. J. *Nature (London)* **1964**, *202*, 83-84.
(49) Brown, W. D.; Merine, L. B. *J. Biol. Chem.* **1968**, *244*, 6696-6701.
(50) Pulsinelli, P. D.; Perutz, M. F.; Nagel, R. L. *Proc. Natl. Acad. Sci. U.S.A.* **1973**, *70*, 3870-3874.

Consistent Porphyrin Force Field. 3. Out-of-Plane Modes in the Resonance Raman Spectra of Planar and Ruffled Nickel Octaethylporphyrin

Xiao-Yuan Li,[†] Roman S. Czernuszewicz,[†] James R. Kincaid,[‡] and Thomas G. Spiro*,[†]

Contribution from the Department of Chemistry, Princeton University, Princeton, New Jersey 08544, and Department of Chemistry, Marquette University, Milwaukee, Wisconsin 53233. *Received November 14, 1988*

Abstract: Low-temperature (12 K) resonance Raman spectra are reported for tetragonal and triclinic crystallites of nickel octaethylporphyrin and its meso-d_4, $^{15}N_4$, and methylene-d_{16} isotopomers. Spectral contributions of the A and B forms in mixed triclinic crystals have been isolated by computer subtraction. The low-frequency (<900 cm^{-1}) spectra contain contributions from in-plane and out-of-plane porphyrin modes. With the aid of a normal-coordinate calculation, a majority of the out-of-plane modes have been assigned and described in terms of local-coordinate contributions. Modes are identified that involve cooperative motions of the pyrrole ring, i.e., tilting, folding, swiveling, and translation. These are implicated in static and dynamic distortions of porphyrin molecules. The ethyl bending coordinates have a major perturbing effect on the out-of-plane frequencies, which will have to be taken into account in extending the analysis to heme proteins. Tentative out-of-plane assignments are also given for nickel tetraphenylporphyrin.

In this paper we develop the first out-of-plane force field for the porphyrin ring based on experimental data. The out-of-plane potential surface is important with respect to the dynamical properties of heme proteins. The heme group is embedded in a protein pocket and is subject to a variety of forces that can distort it from planarity. Such distortions are readily seen in heme protein crystal structures. It is important to know what the restoring forces are in the porphyrin skeleton and how the out-of-plane motions affect the dynamics of, e.g., ligand binding or electron transfer.

The resonance Raman (RR) spectrum is potentially a source of information about these motions,[1] and indeed heme proteins generally display richly detailed RR spectra in the low-frequency region, which may contain bands due to out-of-plane (oop) modes. Marked variations in this region are seen among different proteins, which may well reflect different oop distortions. Thus it is important to have reliable oop assignments to analyze these differences.

The task of assignment is difficult because in the absence of symmetry-lowering effects these modes generally do not appear in the RR spectra. In the ideal D_{4h} symmetry of a metalloporphyrin only the E_g oop modes are Raman allowed (most are "u" modes), and their resonance enhancement requires vibronic

* Author to whom correspondence should be addressed.
† Princeton University.
‡ Marquette University.

(1) Spiro, T. G.; Li, X.-Y. In *Biological Applications of Raman Spectroscopy*; Spiro, T. G., Ed.; Wiley-Interscience: New York, 1988; Vol. III, Chapter 1.

0002-7863/89/1511-7012$01.50/0

mixing between in-plane and out-of-plane electronic transitions ($E_u \times A_{2u} = E_g$).[1] One instance of such activation has been suggested,[2] but vibronically coupled out-of-plane electronic transitions are not generally available for enhancement. The RR spectra are dominated by modes that are enhanced via the in-plane $\pi-\pi^*$ transitions.

We have discovered, however, that many oop modes are activated in nickel octaethylporphyrin (NiOEP) crystals, thanks to symmetry-lowering effects. Tetragonal crystals[3] have a ruffled porphyrin ring, and this distortion is quite effective in allowing RR enhancement of oop modes. Triclinic crystals[4,5] contain forms with planar porphyrin and are less effective in this regard, but the out-of-plane orientation of the ethyl groups does activate a few oop modes. Assignments were made possible by the availability of $^{15}N_4$, meso-d_4, and methylene-d_{16} isotope shifts and by the sharp spectra that were obtainable at low temperature.

An oop force field has been constructed to account for these bands and their isotope shifts. We expect this force field to be useful in analyzing heme protein oop modes. Warshel and Lappicerella[6a] performed a QCFF/PI calculation of the oop modes of a metalloporphine, without, however, recourse to experimental data. Abe[6b] has recently calculated some NiOEP oop modes, using an empirical diagonal force field to account for some of the low-frequency IR bands.

The calculated eigenvectors give insight into the nature of the oop modes. Of particular interest is the A_{2u} mode at 360 cm^{-1}, in which the pyrrole rings tilt in the same direction, producing a doming motion of the porphyrin. This mode has been shown[7] to interact strongly with the asymmetric axial ligand mode of $[(ImH)_2Fe^{III}OEP]^+$ (ImH = imidazole). It may be a determinant of the ligand dissociation dynamics in heme proteins. Another mode of interest is the B_{1u} mode at 612 cm^{-1}, which involves the pyrrole twisting distortion seen in the tetragonal crystal structure.[3] As discussed in the following paper,[8a] this mode is believed to soften in solution, leading to a distribution of ruffled structures along the B_{1u} coordinate.

Experimental Section

Materials and Spectroscopic Measurements. NiOEP and its isotopomers were prepared as described in ref 8b. Tetragonal crystals were formed by quickly evaporating a CS_2 solution of NiOEP. This method is much faster than the benzene/dichloromethane method described in ref 3. Sometimes the tetragonal crystals obtained from this procedure were contaminated with small amounts of triclinic crystals. These can be converted fully to the tetragonal form by high-power laser heating or by directly heating the contaminated sample in an oven at ~250 °C for 30 min as described in ref 9. The purity of the tetragonal crystals was checked by examining the ν_{10} band with 568.2-nm excitation. This mode is at 1642 cm^{-1} for tetragonal crystals but at 1663 cm^{-1} for triclinic crystals.

Triclinic crystals prepared by slow evaporation of a cooled (4 °C) CH_2Cl_2 solution of NiOEP are a mixture of A and B forms,[5] the proportions varying from one preparation to another (as revealed by the RR spectra themselves; vide infra). It was possible to prepare nearly pure B form by the pyridine/dioxane method,[4] but we were unable to produce a pure A form sample. Brennan et al.[5] report that the A form is favored by the presence of free-base OEP to seed the crystals. We were constrained from adding free-base OEP because its fluorescence swamps RR spectra with Q-band excitation and its RR scattering interferes with an already complex NiOEP RR spectrum obtained with B band excitation.[8b] We were able, however, to assign the A form bands by subtracting the B form spectrum from the spectrum of a mixture. The triclinic crystals are unstable and slowly convert to tetragonal crystals upon standing. (After 2 weeks a sample gave a spectrum showing a 70/30% mixture of triclinic and tetragonal forms.) Consequently RR spectra of triclinic crystals were obtained immediately after preparation. The preparation of NiTPP samples is described in ref 8c.

Samples were prepared as KCl pellets, and RR spectra were collected at room temperature with a rotating sample holder[10] and at low temperature (12 K) with a cryogenic sample holder[10] connected to a Model CSA-202E Displex closed-cycle liquid He refrigerator (Air Products, Allentown, PA). Excitation radiation for RR measurements was provided by a Spectra Physics 171 Kr^+ laser. The scattered light was dispersed by a Spex 1401 double monochromator and detected by a cooled RCA 31034A photomultiplier tube using an ORTEC 9315 photon-counting system, under the control of a MINC II (DEC) minicomputer.

Normal-Coordinate Analysis. Normal-mode calculations for a 61-atom metalloporphyrin model used in our out-of-plane (oop) mode analysis were performed with the **GF** matrix method[11a] and a valence force field. The 16 methylene (NiOEP) and 24 methyl (NiOMP) hydrogen atoms were included explictly in the calculation; the methyl groups in NiOEP were treated as 15 amu point masses. Cartesian coordinates for both molecules were generated from structural parameters adopted from NiOEP X-ray crystallographic data[3-5] with small modifications to maintain D_{4h} symmetry for the porphyrin skeleton. For the NiOEP calculations all ethyl groups were oriented with methyls pointing out of the porphyrin plane; the overall symmetry was either D_{2d} or D_4 (see Discussion). The final Cartesian coordinates, including atom-numbering scheme and structural parameters, are given in the supplementary material (see the paragraph at the end of the paper). The internal coordinates (R_i), also given in detail in the supplementary material, consisted of angle bending (δ), four-atom torsion (τ), and two types of oop wagging (γ) coordinates. The first is a typical Wilson coordinate[11a] which describes the motion of a terminal atom relative to a given plane (see Figure 13 of the supplementary material). The second one, also a Wilson type, defines the motion of a bridge atom relative to two or more given planes. The former type includes $\gamma(C_mH)$ and $\gamma(C_\beta C_1)$, while the latter type was used to define wagging motions of C_m ($\gamma(C_\alpha C_m)$) and Ni ($\gamma(NiN)$) atoms. The oop motion of the Ni atom can be described in two ways in Schachtschneider's programs:[11b] by two perpendicular pairs of N–Ni–N triatom linear bending coordinates or by four equivalent oop wagging coordinates that share the same head-atom, the central metal. Both methods give three redundant coordinates, and the latter method was chosen because it has the advantage of defining the oop metal motion relative to four pyrrole rings.

There is a debate in the literature about the best way of defining torsional motions, particularly for the molecules with cyclic ring structures. Some workers have developed torsion force constants based on a four-atom torsion (δ type or τ),[12a,13b] while the others advocate the use of a six-atom torsion (ϕ type).[13g,h] Unfortunately, the force constants associated with the two types of torsions cannot be directly compared. The main reasons for favoring a six-atom torsion is that it results in larger diagonal but smaller interaction force constants,[13g,h] and it can be directly related to the π-bond order of the molecule.[13i] However, it can be shown from the original work of Bell,[13g] who first introduced the six-atom torsion, that it combines two four-atom torsions sharing the same central bond, thereby leading to increased diagonal and decreased interaction force constants. Hence it is a mathematical transformation that produces the appealing numerical properties. The disadvantage of a six-atom torsion is apparent when one compares oop force fields between benzene

(2) Choi, S.; Spiro, T. G. *J. Am. Chem. Soc.* **1983**, *105*, 3683–3692.
(3) Meyer, E. F., Jr. *Acta Crystallogr.* **1972**, *B28*, 2162–2167.
(4) Cullen, D. L.; Meyer, E. F., Jr. *J. Am. Chem. Soc.* **1974**, *96*, 2095–2102.
(5) Brennan, T. D.; Scheidt, W. R.; Shelnutt, J. A. *J. Am. Chem. Soc.* **1988**, *110*, 3919–3924.
(6) (a) Warshel, A.; Lappicirella, A. *J. Am. Chem. Soc.* **1981**, *103*, 4664–4673. (b) Abe, M. In *Spectroscopy of Biological Systems*; Clark, R. J. H., Hester, R. E., Eds.; Wiley: New York, 1986; Vol. 13, Chapter 7.
(7) Mitchell, M.; Li, X-Y.; Kincaid, J. R.; Spiro, T. G. *J. Phys. Chem.* **1987**, *91*, 4690–4696.
(8) (a) Czernuszewicz, R. S.; Li, X.-Y.; Spiro, T. G. *J. Am. Chem. Soc.*, following paper in this issue. (b) Paper 2 of this series: Li, X.-Y.; Czernuszewicz, R. S.; Kincaid, J. A.; Stein, P.; Spiro, T. G. *J. Phys. Chem.*, in press. (c) Paper 1 of this series: Li, X.-Y.; Czernuszewicz, R. S.; Kincaid, J. R.; Su, O.; Spiro, T. G. *J. Phys. Chem.*, in press.
(9) Scheuermann, W.; Nakamoto, K. *J. Mol. Struct.* **1978**, *48*, 285–288.
(10) Czernuszewicz, R. S. *Appl. Spectrosc.* **1986**, *20*, 571–573.
(11) (a) Wilson, E. B.; Decius, J. C.; Cross, P. C. *Molecular Vibrations*; McGraw-Hill: New York, 1955. (b) Schachtschneider, J. M. Shell Development Co., Technical Reports No. 57–65 and 231–264, 1962.
(12) (a) Pulay, P.; Fogaravi, G.; Boggs, J. E. *J. Chem. Phys.* **1981**, *74*, 3999–4014. (b) Pongor, G.; Fogarasi, G.; Boggs, J. E.; Pulay, P. *J. Mol. Spectrosc.* **1985**, *114*, 445–453. (c) Xie, Y.; Fan, K.; Boggs, J. E. *Mol. Phys.* **1986**, *58*, 401–411. (d) Niu, Z.; Dunn, K. M.; Boggs, J. E. *Mol. Phys.* **1985**, *55*, 421–432.
(13) (a) Duinker, J. C.; Mills, I. M. *Spectrochim. Acta* **1968**, *24A*, 417–435. (b) La Lau, C.; Snyder, R. G. *Spectrochim. Acta* **1971**, *27A*, 2073–2088. (c) Scherer, J. R. *Spectroschim. Acta* **1967**, *23A*, 1489–1497; *Ibid.* **1968**, *24A*, 747–770. (d) Scott, D. N. *J. Mol. Spectrosc.* **1969**, *31*, 451–463; *Ibid.* **1971**, *37*, 77–91. (e) Orza, J. M.; Escribano, R.; Navarro, R. *J. Chem. Soc., Faraday Trans. 2* **1985**, *81*, 653–662. (f) Acevedo-Gonzalez, C. A.; Campos-Vallette, M.; Clavigo-Campos, R. E. *Spectrochim. Acta* **1986**, *42A*, 919–925. (g) Bell, R. P. *Trans. Faraday Soc.* **1945**, *41*, 293–295. (h) Kydd, R. A. *Spectrochim. Acta* **1971**, *27A*, 2067–2072. (i) Anno, T. *J. Chem. Phys.* **1958**, *28*, 944–949.

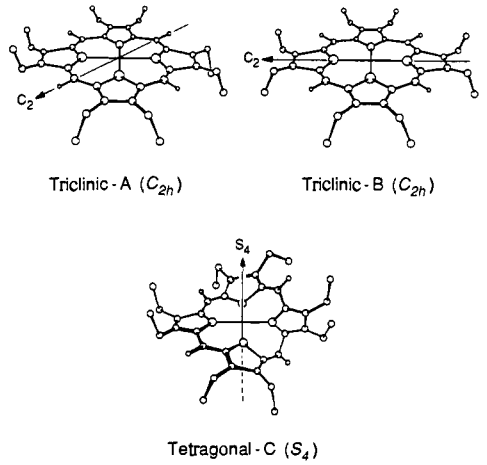

Figure 1. Structural diagram of NiOEP showing ruffled and flat porphyrin rings in the known crystal structures of tetragonal (C)[3] and the two triclinic forms (A and B).[4,5]

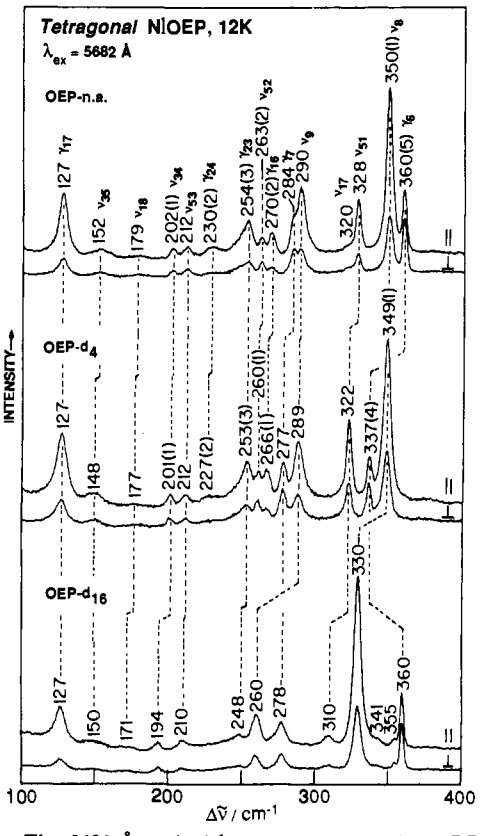

Figure 2. The 5682-Å excited low-temperature (12 K) RR spectra (100–400 cm^{-1}) of tetragonal NiOEP and its meso-d_4 and methylene-d_{16} isotopomers in KCl pellets. ^{15}N shifts are given in parentheses. Band assignments are indicated by the labels. Conditions: 150-mW laser power, 3-cm^{-1} slit width, single scan, 0.5 cm^{-1} increments, 1-s integration time.

and pyridine, since the torsion force constant around N–C bonds cannot be defined by a six-atom type. This point has been discussed by Pulay and co-workers,[12a] who used four-atom torsion in their scaled ab initio calculations of oop force fields for small ring molecules. Because of their greater generality we have used four-atom torsions in developing our porphyrin oop force field. To minimize the number of torsions, we used only cis configurations with respect to a given central bond. Several possible trans torsions (e.g., around N–C_α bonds) can be generated by taking linear combinations of already defined cis torsions and waggings.

The symmetry coordinates (S_i) for NiOEP (D_{2d} and D_4) and NiOMP (D_{2d}) were taken as symmetry-adapted linear combinations of respective internal coordinates (R_i). The corresponding U matrices (S = UR) which contain unnormalized linear transformation coefficients are given in the supplementary material. (Those coefficients can easily be normalized by

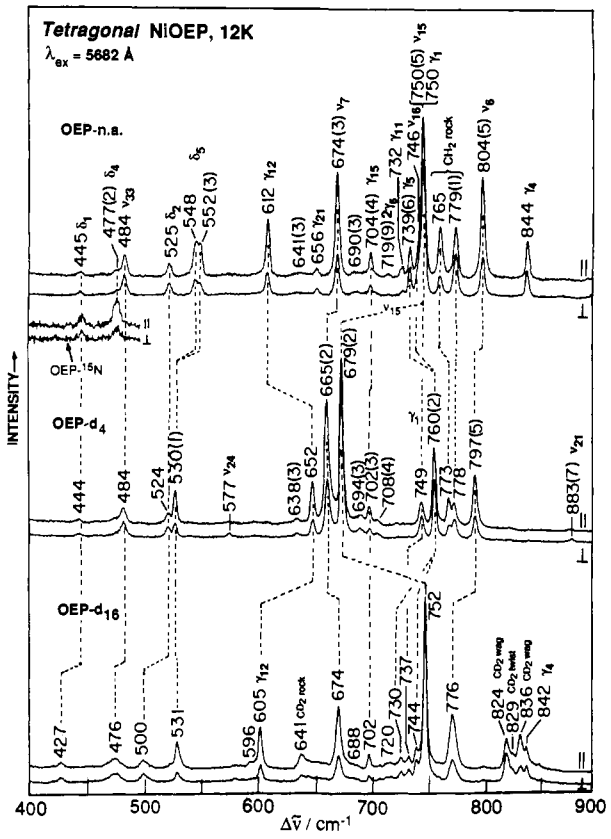

Figure 3. As for Figure 1, but in the 400–900-cm^{-1} region. The inset shows enhancement of the 477-cm^{-1} band with 4067-Å excitation.

standard procedures described in ref 11b.)

The potential energy was expressed by a general valence force field that included R_i-related diagonal (H, γ, and τ) and valence interaction (f) force constants (see Figure 13 of the supplementary material for detailed definitions). The interaction force constants included only those adjacent internal coordinates that share at least one atom or are separated by no more than one bond. Because there are two possible signs for each torsion force, all symmetrically equivalent internal torsion coordinates must be defined in a consistent way, as is illustrated in Figure 13 (supplementary material). The wagging–torsion interactions are directly related to the sign of the torsion force, and the same care in sign convention must be followed in setting up the force field matrices. Torsion–torsion interactions, although included in the **F** matrices, were all set as zero in the final calculations. Schachtschneider's programs[11b] were used to construct the **G** matrices and to solve the secular equations, $|\mathbf{GF} - E\lambda| = 0$, for each symmetry species on a VAX-II/780 computer. The initial force constants were taken from previous oop analyses on benzene, toluene, and other small-ring molecules[12,13] and then adjusted to fit the observed frequencies in the A_{2u} (D_{4h} symmetry notation) block for which the experimental assignments are the most secure. No attempts to refine the force constants were made at this point, but particular attention was paid to reproducing the observed NiOEP meso-H/D, pyrrole-$^{15/14}$N, methylene-H/D, and $^{62/58}$Ni isotope shifts.

Results

Figure 1 contains structural diagrams for the three NiOEP crystal forms examined in this study. NiOEP crystallites give rise to numerous RR bands in the low-frequency region of the spectrum. To resolve these, we cooled the samples to 12 K and obtained sharp spectra with low backgrounds, as illustrated in Figures 2 and 3, which contain 100–400- and 400–900-cm^{-1} 568.2-nm excited spectra of tetragonal crystals[4] (form C, ruffled porphyrin[8b]) of NiOEP and its meso-d_4 and methylene-d_{16} isotopomers. Equally good $^{15}N_4$ isotopomer spectra were obtained, and the ^{15}N shifts are given in parentheses. Because the solid samples were strongly absorbing, reliable polarization measurements could be obtained.[14] The peak frequencies, polarizations, and isotope shifts are listed in Table I. Figure 4 shows the effect

(14) Strommen, D. P.; Nakamoto, K. *Appl. Spectrosc.* **1983**, *37*, 436–439.

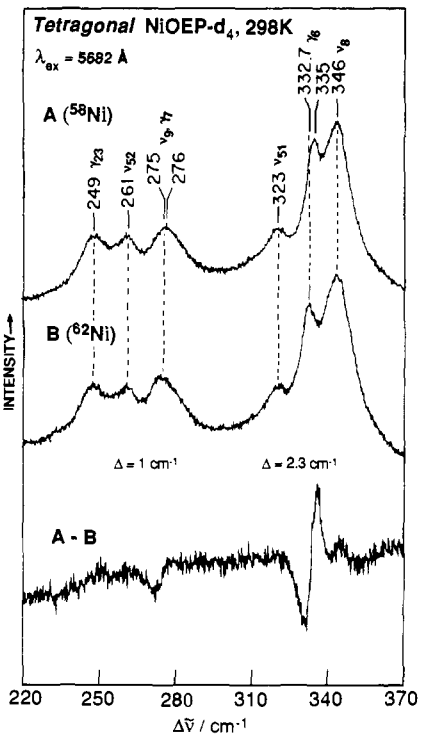

Figure 4. The 5682-Å excited room-temperature RR spectra (220–370 cm^{-1}) of tetragonal NiOEP-d_4 (KCl pellets) with ^{58}Ni and ^{62}Ni. The difference spectrum shows the isotope shifts for the 335- and 276-cm^{-1} bands. Conditions: 150-mW laser power, 4-cm^{-1} slit width, 0.2-cm^{-1} increments, 2-s integration time.

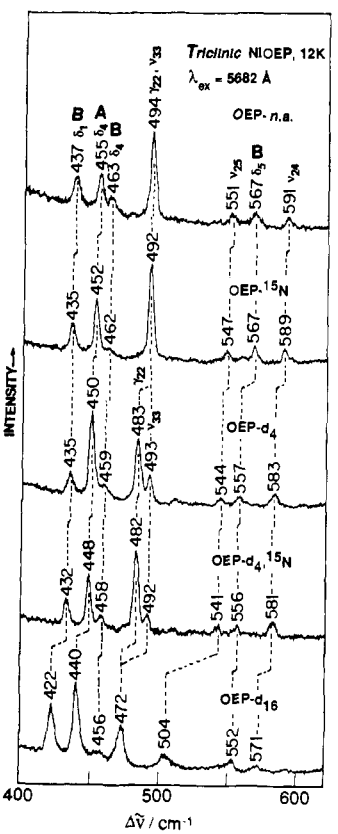

Figure 5. The 5682-Å excited low-temperature (12 K) RR spectra (400–600 cm^{-1}) of triclinic NiOEP and its $^{15}N_4$, meso-d_4, meso-d_4 + $^{15}N_4$, and methylene-d_{16} isotopomers in KCl pellets. Bands corresponding to the A and B forms in the mixed crystals are indicated. Conditions are as in Figure 1.

of ^{62}Ni substitution on the room-temperature tetragonal crystal RR spectrum; the meso-d_4 isotopomer was used in this experiment

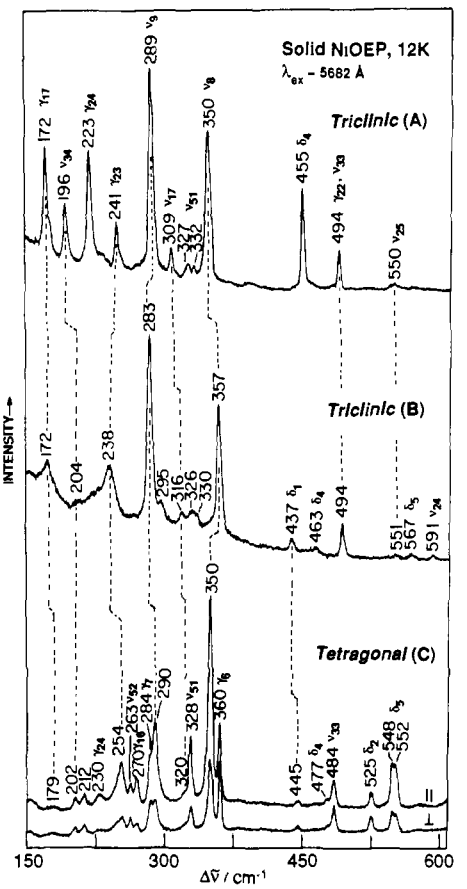

Figure 6. Comparison of 5682-Å excited RR spectra (150–600 cm^{-1}) for tetragonal NiOEP (form C) with computer-deconvoluted spectra of triclinic forms A and B. Conditions are as in Figure 1.

to shift the 360-cm^{-1} γ_6 band (vide infra) to 335 cm^{-1}, away from the strong ν_8 band at 348 cm^{-1}. The γ_6 band is seen to show a 2.3-cm^{-1} ^{62}Ni shift. A 1-cm^{-1} shift is also seen for the 276-cm^{-1} band, assigned to γ_7.

Figure 5 shows a portion of the 568.2-nm excited spectra obtained for triclinic crystals containing a mixture of structures A[4] and B[5] (flat porphyrins but with different ethyl orientations, Figure 1). As we demonstrated previously[8b] the proportions of A and B can be determined from the intensity ratio of the ν_8 bands at 357 and 350 cm^{-1} (see Figure 10 of ref 8b), the frequencies having been determined in A and B single crystals by Brennan et al.[5] Several other bands correlate in intensity with the 357- and 350-cm^{-1} ν_8 bands, and some of them are well resolved. It is therefore straightforward to separate the A and B spectra by computer subtraction to a flat base line by using the A/B ratio as a variable. Results of this procedure are shown in Figures 6 and 7, where the A, B, and C (tetragonal) spectra are compared. Because the triclinic samples were not as deeply colored as the tetragonal ones, the band polarizations are not as pronounced, and only prallel components are displayed in Figures 5–8 for triclinic crystal spectra; nevertheless, the state of polarization could be determined qualitatively. The A and B frequencies and isotope shifts are listed in Table I. In most cases they can be correlated with bands of structure C, although appreciable frequency shifts are observed. Figure 8 is an expanded view of the complicated 750-cm^{-1} region of the spectra and shows how ^{15}N substitution reveals the presence of an oop mode, γ_1, at 750 cm^{-1}, which is present in the tetragonal but missing in the triclinic crystal spectra. Finally, Figure 9 presents 300–900-cm^{-1} region RR spectra of tetragonal crystals with excitation at 406.7 (B-band) and 530.9 and 568.2 nm (Q-bands).

As indicated in Table I, several of the bands are assigned to in-plane porphyrin modes (ν_i) on the basis of their agreement in frequency and isotope shift patterns with the normal-coordinate calculation described in ref 8b. Three bands seen only in the C

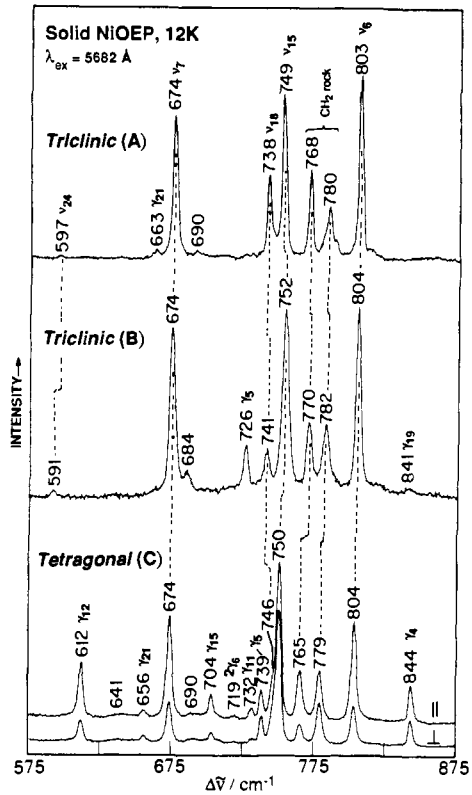

Figure 7. As for Figure 5, but in the 575–875-cm^{-1} region.

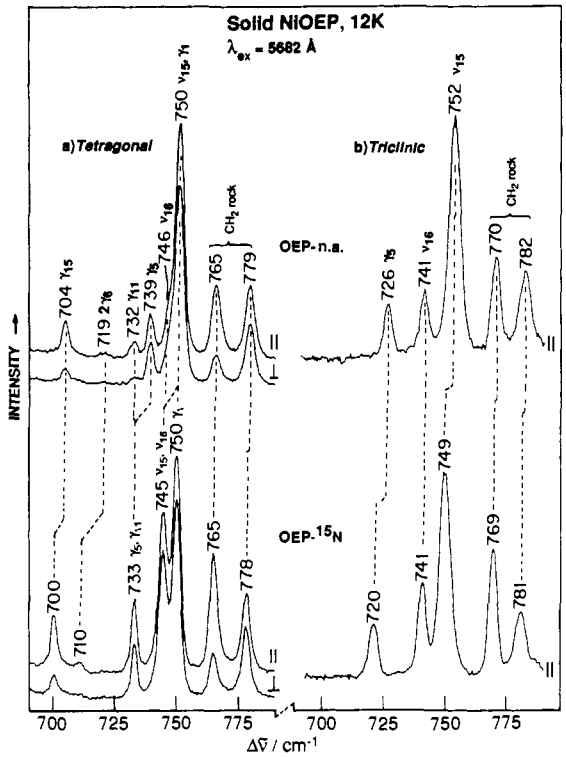

Figure 8. Expanded view of the 750-cm^{-1} region of the 5682-Å excited spectra. The ^{15}N spectra reveal the presence of two modes, ν_{15} and γ_1, under the 750-cm^{-1} band in the tetragonal but not the triclinic crystals.

spectrum, at 212, 263, and 328 cm^{-1}, are assigned to E_u modes: ν_{53}, ν_{52}, and ν_{51}. These IR-active modes gain Raman activity because the symmetry center is lost in the C structure (S_4). They remain inactive in the A and B structures, in which the symmetry center is retained (C_{2h}) (Figure 1). A weak 326/330-cm^{-1} doublet seen in the triclinic crystal spectra, assignable to ν_{51}, may represent a violation of this selection rule, due to solid-state effects.

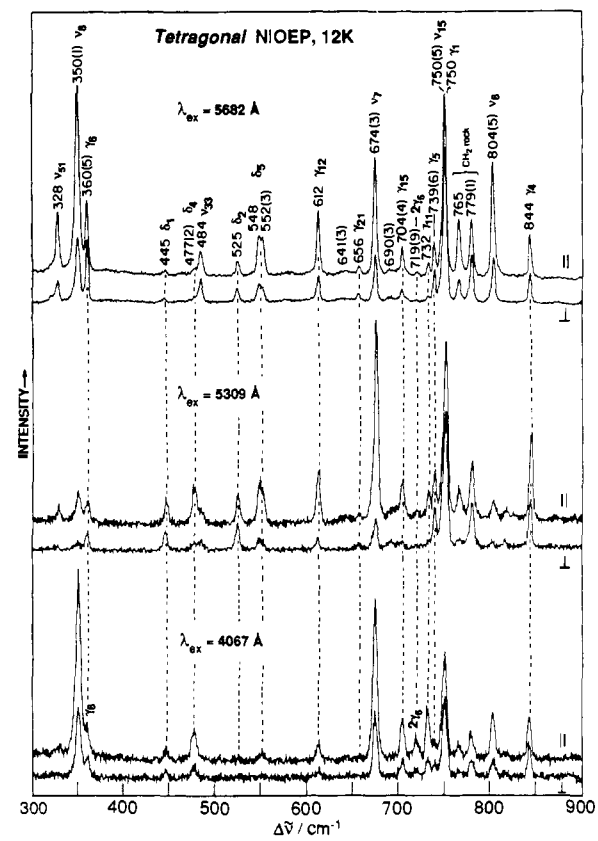

Figure 9. Low-temperature (12 K) RR spectra of tetragonal NiOEP obtained with 5682-, 5309-, and 4067-Å excitations and experimental conditions as in Figure 1. Vertical lines mark out-of-plane modes.

We were able to assign the remaining bands to oop modes, with the aid of the isotope shifts and of a normal-coordinate analysis to secure the identifications. Force constants were selected from published analyses of aromatic molecule out-of-plane modes[12,13] and were altered somewhat to permit reasonable agreement with the observed frequencies and isotope shifts. Details of the force field and internal coordinates are given in the supplementary material. The final force constants are listed in Table II.

Even though ruffled NiOEP, structure C, provided most of the data for the analysis, the porphyrin used for the calculation had a flat skeleton. A ruffled porphyrin model would have required the inclusion of the in-plane as well as the out-of-plane force field, complicating the calculation considerably. Because the actual degree of ruffling in NiOEP is relatively small,[3] the interaction of in-plane and out-of-plane forces should not perturb the out-of-plane mode frequencies and compositions seriously. Where out-of-plane modes are detected in both ruffled and flat NiOEP, the frequency differences are not large (Table I). In addition the IR spectra of triclinic crystals show the A_{2u} modes γ_4 and γ_6 at essentially the frequencies given in Table III. Nevertheless, appreciable deviations between experimental and calculated frequencies were encountered for some of the modes and may reflect the actual difference in geometry. The average discrepancy, 5%, is weighted by large deviations in the B_{2u} block, 11 and 13% for γ_{15} and δ_4.

The ethyl substituents were modeled according to their orientation in the tetragonal crystals,[3] i.e., with the methyl groups pointing alternately up and down on adjacent pyrrole rings (Figure 1), thereby maintaining D_{2d} symmetry (see Figure 1 of ref 8b). This point group has the advantage that the D_{4h} symmetry labels are retained, except for the g and u labels. The methylene H atoms were included explictly in the calculation, but the methyl group was approximated as a 15 amu point mass. Table III compares observed and calculated frequencies. We note that the predicted shifts upon methylene-d_{16} substitution are all zero. This results from the fact that the CH_2 bending motions are parallel to the porphyrin plane when the ethyl $C_\beta C_1 C_2$ planes are perpendicular

Table I. Low-Frequency RR Bands and ^{15}N Isotope Shifts (cm^{-1}) for Tetragonal (C) and Triclinic (A and B) Crystalline Forms of NiOEP and Its Meso-d_4 and Methylene-d_{16} Isotopomers[a]

	tetragonal			triclinic[b]			
ρ	na	meso-d_4	met-d_{16}	na	meso-d_4	met-d_{16}	assgnt[c]
dp	844 (0)		842				γ_4, A_{2u}
ap				841 (0)		841	γ_{19}, E_g
p	804 (5)	797 (5)	776	804 (4) [803]	798 (5)	780	ν_6, A_{1g}
dp	779 (1)	778 (0)		782 (2) [780]	781 (1)		CH_2 rock, B_1
p	765 (0)	773 (0)	641	770 (1) [768]	773 (1)	648	CH_2 rock, A_1
dp	750 (0)[d]	749 (0)	737[e]				γ_1, A_{1u}
dp	750 (5)[d]	679 (2)	752	752 (3) [749]	683 (5)	755	ν_{15}, B_{1g}
dp	746 (0)	760 (2)[d]	744[e]	741 (0) [738] [0]	757 (1) [764] [2]	734	ν_{16}, B_{1g}
dp	739 (6)	760 (2)[d]	730	726 (6)	732 (4)	726	γ_5, A_{2u}
p	732 (0)						γ_{11}, B_{1u}
p	719 (9)		720				$2\gamma_6$
p	704 (4)	702 (3)	702				γ_{15}, B_{2u}
dp	690 (3)	694 (3)	688	684 (3) [690]	700 (3)		?
p					712 (3)		?
dp					688 (0)		?
p	674 (3)	665 (2)	674	674 (2)	668 (2)	673	ν_7, A_{1g}
dp	656 (0)			663 (0)			γ_{21}, E_g
dp	641 (3)	638 (3)			633 (3) [638] [3]		?
p	612 (0)	652 (0)	605				γ_{12}, B_{1u}
p			596				?
ap		577 (0)		591 (2) [597]	583 (2)	571	ν_{24}, A_{2g}
p	552 (3)/548 (0)	530 (1)	531	567 (0)	557 (1)	552	δ_5, E_g
ap				551 (4)	544 (3)	504	ν_{25}, A_{2g}
dp	525 (0)	524 (0)	500				δ_2, A_{2u}
dp				494 (2)[d]	483 (1)	472[d]	γ_{22}, E_g
dp	484 (0)	484 (0)	476	494 (2)[d]	493 (1)	472[d]	ν_{33}, B_{2g}
p	477 (2)	477 (2)		463 (1) [455] [3]	459 (1) [450] [2]	456 [440]	δ_4, B_{2u}
dp	445 (0)	444 (0)	427	437 (2)	435 (3)	422	δ_1, A_{1u}
dp	360 (5)	337 (4)	360				γ_6, A_{2u}
dp			355[e]				ν_{50}, E_u
p	350 (1)	349 (1)	330	357 (1) [350] [0]	353 (1) [350] [0]	342 [321]	ν_8, A_{1g}
p	328 (0)	322 (0)	310	330 (0)/326 (0) [332]/[327]	324 (0)	327/321	ν_{51}, E_u
dp	320 (0)			316 (0) [309]	314 (0)		ν_{17}, B_{1g}
p						310	?
dp				295 (0)	293 (0)		?
p	290 (0)	289 (0)	260[d]	283 (2) [289] [1]	282 (3) 289 [1]	272 [281]	ν_9, A_{1g}
dp	284 (0)	277 (0)	278				γ_7, A_{2u}
p	270 (2)	266 (1)	260[d]				γ_{16}, B_{2u}
dp	263 (2)	260 (1)	260[d]				ν_{52}, E_u
p	254 (3)	253 (3)	248	241 (2) [238]	241 (2)	236	γ_{23}, E_g
p	230 (2)	227 (2)	210[d]	223 (2)	222 (2)	221/216	γ_{24}, E_g
dp	212 (0)	212 (0)	210[d]				ν_{53}, E_u
dp	202 (1)	201 (1)	194	204 (0) [196] [0]	204 (0) [194] [1]	195 [190]	ν_{34}, B_{2g}
dp	179 (0)	177 (0)	171	172 (0)	170 (0)	168	ν_{18}, B_{1g}
dp	152 (0)	148 (0)	150	143 (0)	140 (0)	143	ν_{35}, B_{2g}
p	127 (0)	127 (0)	127				γ_{17}, B_{2u}

[a] Observed values from KCl pellet RR spectra at 12 K. na = natural abundance; meso-d_4 and met-d_{16} = ^2H substituted analogues at methine carbon and methylene group positions, respectively. Pyrrole ^{15}N isotope shifts for na and meso-d_4 molecules are given in parentheses; not available for the met-d_{16} isotopomer. [b] Most frequencies are common to the A and B forms; where separate bands are seen, the A form frequency is given in brackets below the corresponding B form frequency. [c] See Table III (γ_i and δ_i) and ref 8b (ν_i) for mode descriptions. [d] Overlapping bands. [e] Tentative assignments.

to the porphyrin plane. In the actual triclinic structure[3] the angles between the planes deviate from 90° by up to 10°. We attribute the observed d_{16} sensitivity of some of the modes to the resulting involvement of CH_2 bending character.

With this analysis in hand we reexamined the low-frequency RR spectra of nickel tetraphenylporphyrin (NiTPP),[8c] whose crystal structure is reported to be isomorphous with that of CuTPP, which shows appreciable porphyrin ruffling.[15a] Excitation at 5682 Å brings out many low-frequency bands, as shown in Figure 10. Some of these are in-plane (ν_i) and phenyl modes (ϕ_i, π_i),[8c] but

(15) (a) Fleischer, E. B.; Miller, C. K.; Webb, L. E. *J. Am. Chem. Soc.* **1964**, *86*, 2342–2347. (b) Burger, H.; Burczyk, K.; Fuhrhop, J. M. *Tetrahedron* **1971**, *27*, 3257–3261.

Table II. Valence Force Constants (mdyn Å/rad²) for Out-of-Plane Vibrations of NiOEP

principal force const[a]		interaction force const[b]	
$\gamma(C_mH)_1 = 0.330$			
$\gamma\ (C_\alpha C_m)_2 = 0.400$	$\mathbf{f}(\gamma_i,\gamma_j)$	$f(1,2) = 0.030$	$f(1,4) = -0.040$
$\gamma(C_\beta C_1)_3 = 0.420$		$f(2,2) = 0.020$	$f(2,3) = 0.030$
$\gamma(NiN)_4 = 0.240$		$f(2,4) = 0.020$	$f(3,3) = -0.020$
		$f(3,4) = -0.030$	$f(4,4) = 0.070$
$\tau(C_\beta C_\beta)_1 = 0.190$			
$\tau(C_\alpha C_\beta)_2 = 0.190$	$\mathbf{f}(\gamma_i,\tau_j)$	$f(1,3) = -0.065$	$f(2,1) = 0.040$
$\tau(C_\alpha C_m)_3 = 0.210$		$f(2,2) = -0.060$	$f(2,3) = \pm 0.025$[d]
$\tau(NC_\alpha)_4 = 0.210$		$f(2,4) = 0.060$	$f(3,1) = -0.040$
$\tau(C_\beta C_1)_5 = 0.0003$[c]		$f(3,2) = 0.070$	$f(3,3) = 0.020$
		$f(3,4) = 0.020$	$f(4,2) = 0.025$
$H(C_\beta C_1 C_2)_1 = 0.900$		$f(4,3) = -0.030$	$f(4,4) = -0.030$
$H(HC_1H)_2 = 0.540$			
$H(C_\beta C_1 H)_3 = 0.625$	$\mathbf{f}(H_k,\gamma_j)$	$f(1,3) = -0.080$	
$H(C_2C_1H)_4 = 0.625$			

[a] γ_i and τ_j are principal out-of-plane wagging and dihedral angle torsion force constants for the indicated bonds. H_k is the ethyl internal angle bending force constant. The subscripted numbers are used to label the interaction force constants. [b] Interaction force constants are included only for wagging–wagging and wagging–torsion interactions. Torsion–torsion interactions were found to have neglibible effect on the calculated frequencies and were set as zero. [c] This force constant describes the ethyl rotation around the C_β–C_1 bond. Its value corresponds to a rotational barrier of 8–10 kcal/mol for a single ethyl group. Moderate variations of this value were found to have no effect on the results. [d] Plus and minus signs correspond to the wag–torsion interactions between $\gamma(C_\alpha C_m)_2$ and $\tau(C_\alpha C_m)_3$ sharing three and two common atoms, respectively.

several can be assigned to out-of-plane modes on the basis of their isotope shifts and by analogy with NiOEP. Table IV lists all the NiTPP low-frequency RR bands and their isotope shifts which are candidates for oop modes.

Discussion

Out-of-Plane Mode Description. Porphyrin oop vibrations occur in the frequency region below 1000 cm⁻¹, since they involve only bending and torsion coordinates. If the peripheral substituents are treated as point masses, there are 34 out-of-plane vibrations, which classify as

$$\Gamma_{oop} = 3A_{1u} + 6A_{2u} + 5B_{1u} + 4B_{2u} + 8E_g$$

in the D_{4h} point group. Among these modes only those with E_g symmetry are Raman-active. In RR scattering, the E_g modes, being non-totally symmetric, require vibronic (B term) activation.[1] Moreover, they must mix an out-of-plane (A_{2u}) with an in-plane (E_u) electronic transition since $E_g = E_u \times A_{2u}$. The vibronic mixing of the in-plane Q and B transitions, which is responsible for the activation of the in-plane non-totally symmetric modes (B_{1g}, B_{2g}, and A_{2g})[1] cannot active the E_g vibrations (E_g is not contained in the $E_u \times E_u$ product). Infrared activity is carried only by the A_{2u} out-of-plane modes.

Because of these symmetry restrictions, the oop modes have been difficult to characterize, although limited assignments have been suggested.[2,6b] The symmetry lowerings found in the NiOEP crystals[3-5] present an opportunity for more complete characterizations. In triclinic crystals the ethyl orientations impose C_{2h} symmetry for both A and B forms.[8b] Thus the center of symmetry is maintained, and all the **u** modes remain Raman inactive. (But the subscripts 1 and 2 are lost.) The E_g modes, however, correlate with $A_g + B_g$ in the C_{2h} point group. The A_g components are subject to Franck–Condon enhancement, while the B_g components can be activated by Q/B electronic mixing, just as the in-plane B_g modes are.[1] Thus, E_g modes can appear in the triclinic crystal spectra, and five of these, γ_{19}, γ_{21}, γ_{22}, γ_{23}, and γ_{24}, have been identified (Tables I, III, and VI).

In tetragonal crystals the ethyl orientations impose D_{2d} symmetry, and the porphyrin ruffling does also. Because one of these D_{2d} subgroups is rotated by 45° with respect to the other, the overall point group is S_4. The $D_{4h} \rightarrow D_{2d}$ oop correlations are $A_{1u} \rightarrow B_1$, $A_{2u} \rightarrow B_2$, $B_{1u} \rightarrow A_1$, $B_{2u} \rightarrow A_2$, and $E_g \rightarrow E$ for the ruffling distortion, while for the ethyl orientation subgroup the B_{1u} and B_{2u} correlations are reversed: descending from D_{2d} to S_4, B_1, $B_2 \rightarrow B$, A_1, $A_2 \rightarrow A$, and $E \rightarrow E$. The effective symmetry can be determined from the polarization state of the oop modes classifying as B_{1u} and B_{2u} in D_{2h} symmetry; all other modes should be depolarized in all three subgroups. The B_{1u} and B_{2u} modes should be polarized and depolarized, respectively, if the ethyl orientations effect is dominant, and vice versa if ruffling is dominant. In fact all the RR bands assigned to B_{1u} as well as B_{2u} modes are polarized, indicating that both symmetry-lowering mechanisms are active and that the effective symmetry is S_4.

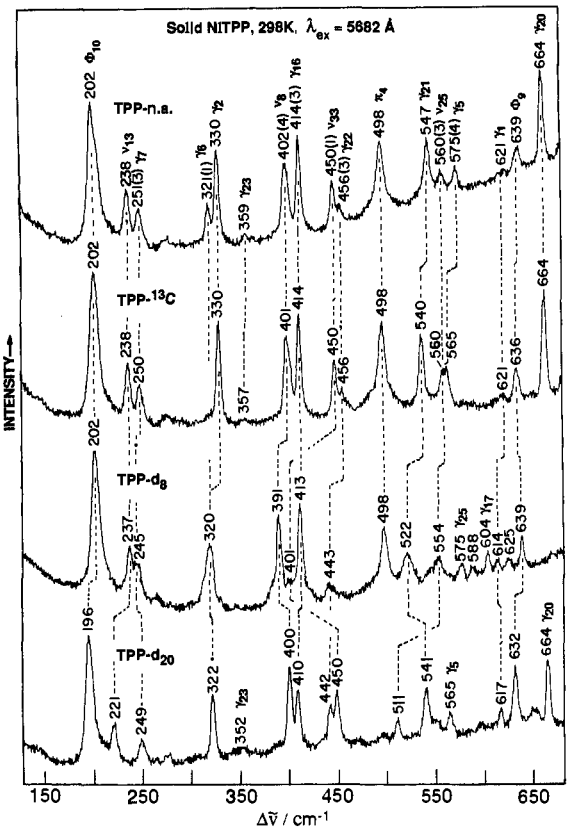

Figure 10. The 5682-Å excited room-temperature RR spectra (100–700 cm⁻¹) of NiTPP and its $^{13}C_4$, d_8, and d_{20} isotopomers,[8b] in KCl pellets. ^{15}N shifts are given in parentheses. Band assignments are indicated by the labels. Conditions: 150-mW laser power, 4-cm⁻¹ slit width, 0.5-cm⁻¹ increments, 2-s integration time.

It is convenient to describe the oop modes qualitatively in terms of local motions of the porphyrin structural elements, i.e., the central metal atom, the C_mH methine bridges, the pyrrole rings, and the peripheral substituents. A set of local motions, introduced by Choi and Spiro,[2] is shown in Figure 11. To these are added the $\delta(C_\beta C_1 C_2)$ ethyl bending coordinates, which couple strongly to the $\gamma(C_\beta C_1)$ coordinate when the ethyl groups are oriented out of the porphyrin plane, as they are in NiOEP. (The C_1C_2 ethyl stretches can also be classified as out-of-plane in this orientation, but these relatively high frequency modes have already been treated in connection with the in-plane plus ethyl force field in our study of the NiOEP in-plane modes.[8b] They are omitted from the present discussion, although the coordinate was included in the calculation.) The six $\delta(C_\beta C_1 C_2)$ modes, found in the 400–550-cm⁻¹ region, perturb the frequencies of neighboring modes quite strongly as shown by comparison with the frequencies calculated for NiOMP (octamethylporphyrin) using the same force field, as shown in Table V.

Table VI lists the NiOEP oop modes, classified according to the local-mode contributions. The numerical entries are the assigned frequencies or, when assignments are unavailable, the calculated ones (in brackets). The major local-mode contribution was judged qualitatively by examining the eigenvectors, shown in Figure 12. Naturally, the local motions mix substantially in

Table III. Calculated and Observed Frequencies and ^{15}N Isotopic Shifts (cm^{-1}) for Out-of-Plane Modes of NiOEP and Its Meso-d_4 Isotopomer[a]

mode	NiOEP ($\Delta^{15}N$) obsd	NiOEP ($\Delta^{15}N$) calcd	NiOEP-d_4 ($\Delta^{15}N$) obsd	NiOEP-d_4 ($\Delta^{15}N$) calcd	description[b]
A_{1u}(B) modes[c]					
γ_1	750 (0)[d]	725 (0)	749 (0)	725 (0)	pyr $fold_{asym}$
δ_1	445 (0)	474 (0)	444 (0)	474 (0)	$\delta(C_\beta C_1 C_2)_{asym}$
γ_2		346 (0)		346 (0)	pyr swivel
γ_3		74 (0)		74 (0)	$\gamma(C_\beta C_1)_{asym}$
A_{2u}(B) modes					
γ_4	844 (0)	829 (1)	681 (3)[e]	667 (6)	$\gamma(C_mH)$
γ_5	739 (6)	736 (6)	760 (2)[d]	763 (1)	pyr $fold_{sym}$
δ_2	525 (0)	562 (1)	524 (0)	561 (1)	$\delta(C_\beta C_1 C_2)_{sym}$
γ_6	360 (5)	351 (5)	337 (4)	310 (4)	pyr tilt
γ_7	284 (0)	263 (1)	277 (0)	256 (0)	$\gamma(C_\alpha C_m)$
γ_8		108 (0)		107 (0)	$\gamma(C_\beta C_1)_{sym}$
γ_9		32 (0)		32 (0)	γ(NiN)
B_{1u}(A) modes					
γ_{10}	853 (0)[f]	845 (0)		501 (0)	$\gamma(C_mH)$
γ_{11}	732 (0)	733 (0)		790 (0)	pyr $fold_{asym}$
γ_{12}	612 (0)	589 (0)	652 (0)	706 (0)	pyr swivel
δ_3		392 (0)		383 (0)	$\delta(C_\beta C_1 C_2)_{asym}$
γ_{13}		130 (0)		125 (0)	$\gamma(C_\alpha C_m)$
γ_{14}		44 (0)		43 (0)	$\gamma(C_\beta C_1)_{asym}$
B_{2u}(A) modes					
γ_{15}	704 (4)	627 (3)	702 (3)	627 (3)	pyr $fold_{sym}$
δ_4	477 (2)	538 (2)	477 (2)	538 (2)	$\delta(C_\beta C_1 C_2)_{sym}$
γ_{16}	270 (2)	253 (3)	266 (1)	253 (4)	pyr tilt
γ_{17}	127 (0)	127 (1)	127 (0)	127 (1)	$\gamma(C_\beta C_1)_{sym}$
γ_{18}		30 (0)		30 (0)	pyr transl.
E_g(E) modes					
γ_{19}	841 (0)[g]	836 (0)		773 (0)	$\gamma(C_mH)$
γ_{20}		731 (0)		712 (0)	pyr $fold_{asym}$
γ_{21}	656 (0)[h]	667 (3)		627 (3)	pyr $fold_{sym}$
δ_5	552 (3)/548 (0)	562 (0)	530 (1)	547 (2)	$\delta(C_\beta C_1 C_2)_{sym}$
γ_{22}	494 (2)[g]	506 (1)	483 (1)[g]	484 (0)	pyr swivel
δ_6		382 (0)		371 (0)	$\delta(C_\beta C_1 C_2)_{asym}$
γ_{23}	254 (3)	244 (3)	253 (3)	243 (2)	pyr tilt
γ_{24}	230 (2)	207 (1)	227 (2)	194 (1)	$\gamma(C_\alpha C_m)$
γ_{25}		91 (1)		91 (1)	$\gamma(C_\beta C_1)_{sym}$
γ_{26}		63 (0)		63 (0)	$\gamma(C_\beta C_1)_{asym}$

[a] Observed values from RR spectra of tetragonal crystals at 12 K. Calculated methylene-d_{16} shifts are all zero, because of the orthogonality of the porphyrin and ethyl planes in the model (see text). Calculated $^{62/58}$Ni shifts are zero except for the four lowest A_{2u}(B) modes; 0.8, γ_6, 0.3, γ_7; 1.6, γ_8; 0.8 cm^{-1}, γ_9. [b] Mode descriptions are based on the eigenvectors presented in Figure 11. Subscripts sym and asym indicate symmetric and asymmetric combinations with respect to the C_2 bisecting the pyrrole rings. [c] Mode symmetry in the D_{4h} (S_4) point group. [d] Overlapping bands (see Table I). [e] These values from KBr pellet IR spectrum at room temperature; in the RR spectrum this position is abscured by ν_{15}. [f] Seen in solution RR spectra.[8e] [g] These values from RR spectra of triclinic crystals at 12 K. [h] Alternative assignment for this mode might be a weak 641-cm^{-1} dp band, which downshifts 3 cm^{-1} in the ^{15}N and meso-d_4 isotopomer spectra (see Table I).

Table IV. Candidate RR Frequencies (cm^{-1}) for the Out-of-Plane Vibrations of NiTPP and its $^{1k}5N_4$, $^{13}C_4$, d_8, and d_{20} Isotopomers[a]

solid NiTPP	solid $^{15}N_4$	solid $^{13}C_4$	solid d_8	solid d_{20}	solid ρ	solution NiTPP	solution ^{15}N	solution ^{13}C	solution d_8	solution d_{20}	solution ρ	assgnt[b]
915	912	914			dp							$\gamma_{26}(E_g)$, $\gamma(C_\beta H)_{asym}$
900	900	901		902	p	904	904	904		904	p	$\gamma_3(A_{1u})$, $\gamma(C_\beta H)_{asym}$
797	797	795	604	797	p	782	777	782	599	779	p	$\gamma_{17}(B_{2u})$, $\gamma(C_{BH})_{sym}$
741	741	733	575	740	dp	737	736	732			dp	$\gamma_{25}(E_g)$, $\gamma(C_\beta H)_{sym}$
712	709	707	554	710	dp							$\gamma_8(A_{2u})$, $\gamma(C_\beta H)_{sym}$
664	664	664		664	p							$\gamma_{20}(E_g)$, pyr $fold_{asym}$
621	621	621	614	617	p							$\gamma_1(A_{1u})$, pyr $fold_{asym}$
605[c]	602[c]	604[c]	594[c]	596[c]	p							$\gamma_{15}(B_{2u})$, pyr $fold_{sym}$
575	571	565		565	dp							$\gamma_5(A_{2u})$, pyr $fold_{sym}$
547	547	540	522	541	p	552	552	543	527	540	p	$\gamma_{21}(E_g)$, pyr $fold_{sym}$
456	453	456	443	442	dp							$\gamma_{22}(E_g)$, pyr swivel
414	411	414	413	410	dp							$\gamma_{16}(B_{2u})$, pyr tilt
359	359	357		352	dp							$\gamma_{23}(E_g)$, pyr tilt
330	330	330	320[d]	322[d]	p	333	332	333	322	327	p	$\gamma_2(A_{1u})$, pyr swivel
321	320		320[d]	322[d]	p							$\gamma_6(A_{2u})$, pyr tilt
251	248	250	245	249	dp	255	251	254	250	255	dp	$\gamma_7(A_{2u})$, $\gamma(C_\alpha C_m)$
165[c]	163[c]		163[c]		p							$\gamma_{24}(E_g)$, $\gamma(C_\alpha C_m)$

[a] Observed values from rotating KCl pellet (solid) and spinning NMR tube (CS_2 solution) RR spectra at room temperature (568.2-nm excitation). $^{15}N_4$ and $^{13}C_4$ = ^{15}N and ^{13}C substituted analogues at the pyrrole nitrogen and methine carbon atom positions, respectively. d_8 and d_{20} = ^2H substituted analogues at the pyrrole C_β and phenyl carbon atom positions, respectively. [b] See Table III for oop mode numbering and descriptions. [c] Seen with 514.5-nm excitation. [d] Overlapping bands.

the normal modes. This mixing is reflected in the spread of frequencies found for a given local mode in Table VI. Nevertheless, because of the high symmetry there are few ambiguities in classifying the modes, even if the eigenvectors are only approximately correct. The mode numbering system parallels that introduced by Kitagawa and co-workers[16] for the in-plane modes.

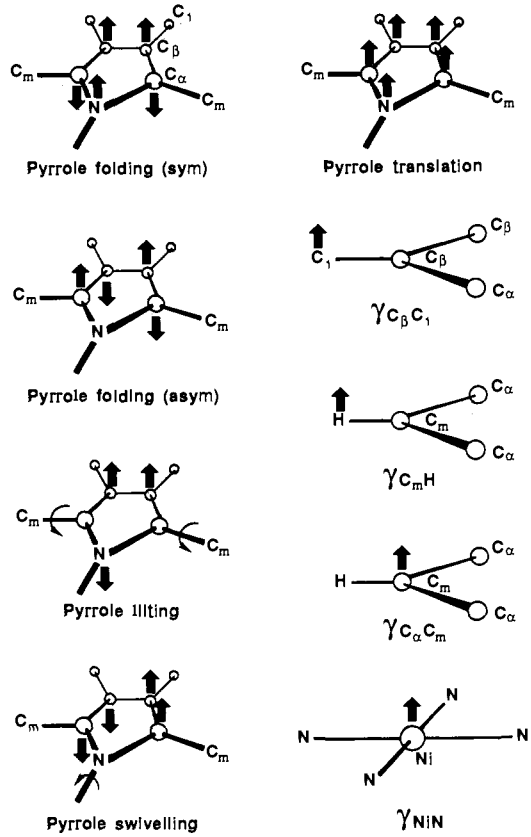

Figure 11. Illustration of local out-of-plane modes used in the classification. Internal ethyl coordinates are not shown but were included in the calculation.

The oop modes are designated γ_i and are numbered in order of descending frequency within each symmetry block in the parent D_{4h} point group, from A_{1u} to A_{2u} to B_{1u} to B_{2u} to E_g. The ethyl bending modes are counted separately, δ_1–δ_6, to facilitate comparison with other porphyrins (e.g., NiOMP, Table V).

We note that several of the oop bands are surprisingly strong in the 5682-Å excited spectra. Thus the pyrrole translation mode γ_{17} at 127 cm^{-1} and the pyrrole tilting mode γ_6 at 360 cm^{-1} are about half as strong as the in-plane mode ν_8, which is the strongest feature in the low-frequency spectrum. Likewise the intensities of the pyrrole swivel mode γ_{12} at 612 cm^{-1} and the $\gamma(C_mH)$ mode γ_4 at 844 cm^{-1} are about half as large as the in-plane modes ν_7 (674 cm^{-1}) and ν_6 (804 cm^{-1}). For the B symmetry modes, γ_4 and γ_6, we surmise that the porphyrin ruffling produces an in-plane component of their eigenvectors that is effective in coupling the Q and B electronic transitions. For the A symmetry modes, γ_{12} and γ_{17}, a substantial Franck–Condon product in the resonant Q state is inferred, due to the out-of-plane components of the transition dipole. γ_{12} is also enhanced with Soret excitation (Figure 9), as is γ_{11}, and the ethyl bending mode δ_4 at 477 cm^{-1} (see also inset of Figure 3). This δ_4 enhancement may be associated with the involvement of the ethyl groups in the NiOEP excited states as discussed in our study of the NiOEP in-plane modes.[8b] NiOEP solutions also show a prominent 466-cm^{-1} polarized band in Soret-excited spectra.

In comparison, the E_g modes are quite weak in the tetragonal crystals, consistent with the lack of an effective enhancement mechanism, the intensity requiring coupling to out-of-plane electronic transitions. Again the ethyl bending mode, δ_5, is exceptional, showing substantial intensity and also a splitting into 548/552-cm^{-1} components, implying an effective symmetry lower than S_4 in this case.

An interesting effect is the appearance of the γ_6 overtone at 719 cm^{-1}, identifiable via its large (9 cm^{-1}) ^{15}N shift, double that

(16) Abe, M.; Kitagawa, T.; Kyogoku, Y. *J. Chem. Phys.* **1978**, *69*, 4526–4534.

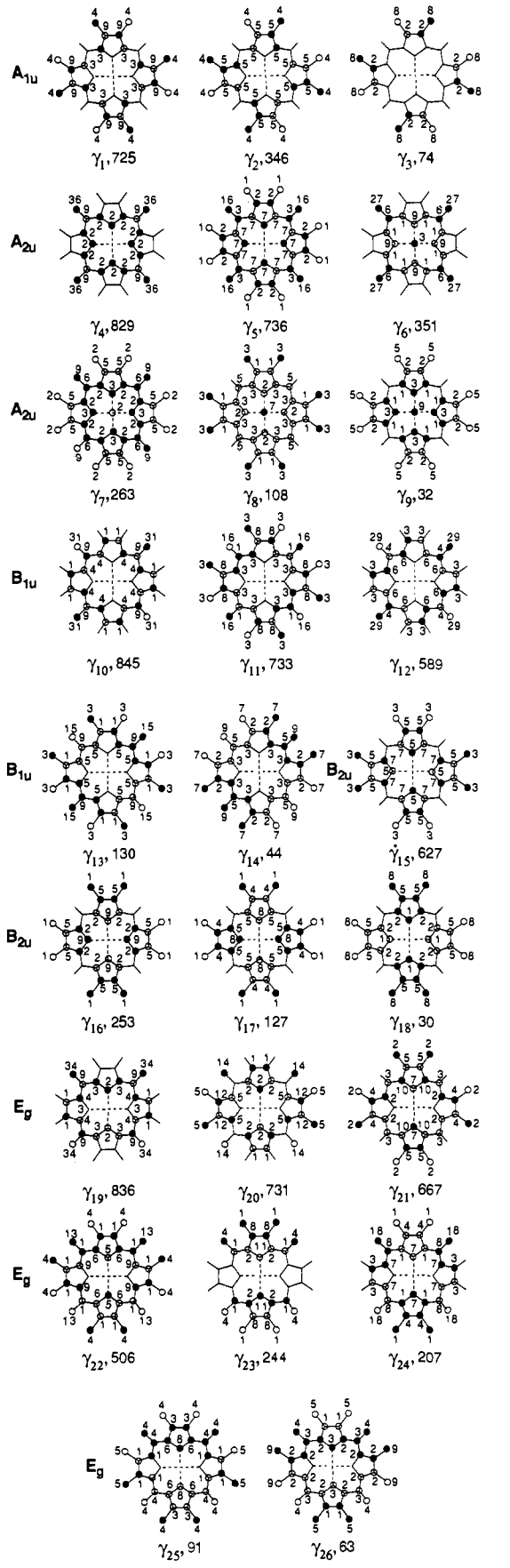

Figure 12. Eigenvectors of the oop modes. The oop direction is indicated by the open (down) and filled (up) circles, and the numbers are the relative displacements of the atoms. Ethyl atoms beyond C_1 are omitted for clarity.

Table V. Calculated Out-of-Plane Mode Frequencies (cm^{-1}) for NiOEP with Different Ethyl Orientations and for NiOMP[a]

mode	NiOEP D_{2d}	NiOEP D_4	description	NiOMP
A_{1u} modes[b]				
γ_1	725	767	pyr $fold_{asym}$	651
δ_1	474	470	$\delta(C_\beta C_1 C_2)_{asym}$	
γ_2	346	334	pyr swivel	407
γ_3	74	74	$\gamma(C_\beta C_1)_{asym}$	93
A_{2u} modes				
γ_4	829	829	$\gamma(C_mH)$	829
γ_5	736	740	pyr $fold_{sym}$	733
δ_2	562	589	$\delta(C_\beta C_1 C_2)_{sym}$	
γ_6	351	351	pyr tilt	360
γ_7	263	254	$\gamma(C_\alpha C_m)$	328
γ_8	108	107	$\gamma(C_\beta C_1)_{sym}$	124
γ_9	32	32	γ(NiN)	34
B_{1u} modes				
γ_{10}	845	847	$\gamma(C_mH)$	845
γ_{11}	733	769	pyr $fold_{asym}$	679
γ_{12}	589	594	pyr swivel	544
δ_3	392	376	$\delta(C_\beta C_1 C_2)_{asym}$	
γ_{13}	130	129	$\gamma(C_\alpha C_m)$	148
γ_{14}	44	44	$\gamma(C_\beta C_1)_{asym}$	50
B_{2u} modes				
γ_{15}	627	647	pyr $fold_{sym}$	608
δ_4	538	548	$\delta(C_\beta C_1 C_2)_{sym}$	
γ_{16}	253	245	pyr tilt	319
γ_{17}	127	126	$\gamma(C_\beta C_1)_{sym}$	144
γ_{18}	30	30	pyr transl.	32
E_g modes				
γ_{19}	836	836	$\gamma(C_mH)$	836
γ_{20}	731	701	pyr $fold_{asym}$	684
γ_{21}	667	652	pyr $fold_{sym}$	635
δ_5	562	538	$\delta(C_\beta C_1 C_2)_{sym}$	
γ_{22}	506	529	pyr swivel	480
δ_6	382	483	$\delta(C_\beta C_1 C_2)_{asym}$	
γ_{23}	244	330	pyr tilt	315
γ_{24}	207	217	$\gamma(C_\alpha C_m)$	216
γ_{25}	91	112	$\gamma(C_\beta C_1)_{sym}$	108
γ_{26}	63	78	$\gamma(C_\beta C_1)_{asym}$	75

[a] See structure models C (D_{2d}) and D (D_4) in Figure 1 of ref 8b for ethyl group orientations. [b] Mode labels are in D_{4h} point group.

of γ_6. Although weak in the 5682- and 5309-Å excited spectra, it becomes as strong as the fundamental when excited at 4067 Å (see Figure 9). Other examples of non-totally symmetric mode overtone enhancement have been seen, e.g., in the case of the asymmetric Fe–O–Fe stretch of a hemerythrin analogue complex.[17]

Assignments. We now discuss the band assignments upon which the above analysis is based, referring to the A, B, and C spectra in Figures 6 and 7 and to the calculation in Table III. D_{4h} symmetry labels are used for clarity, the effects of symmetry lowering having been discussed in the preceding paragraphs. Most of the oop modes, those in the A_{2u}, B_{1u}, and E_g blocks, are markedly sensitive to meso-deuteration (Table III), due to involvement of the C_mH wagging coordinates. These coordinates do not contribute to the A_{1u} and B_{2u} blocks, however, which are d_4-insensitive. We note also that ^{15}N shifts are excluded by symmetry for the A_{1u} and B_{1u} blocks. These restrictions are relaxed in principle when lowering the symmetry from D_{4h}, but the isotope shifts induced by the symmetry lowering should be quite small.

The $\gamma(C_mH)$ modes are expected at ~840 cm^{-1}, as in other aromatics,[18] and two of them can be identified. The fairly strong 844-cm^{-1} mode of C, which disappears in the meso-d_4 spectrum, is assigned to γ_4 (A_{2u}), while the broad weak 841-cm^{-1} bands of A and B are assigned to γ_{19} (E_g). The $\delta(C_\beta C_1 C_2)$ modes are expected near 450 cm^{-1} and are assigned to a series of bands in the 400–550-cm^{-1} region of the C spectrum. In the 640–740-cm^{-1} region one finds a set of bands that are calculated to be pyrrole folding modes. One of these, γ_1, at 750 cm^{-1} is revealed in the ^{15}N spectrum, Figure 8, when the overlapping ν_{15} is shifted to 745 cm^{-1}. Another one, γ_5 at 739 cm^{-1}, is distinguished by its 6-cm^{-1} $^{15}N_4$ downshift and large (21 cm^{-1}) meso-d_4 upshift. This upshift results from the crossing over of the γ_4 C_mH bending mode. These folding modes are pushed up substantially from their expected values[18] of 500–600 cm^{-1} by interaction with the $\delta(C_\beta C_1 C_2)$ modes. Table V shows that the values calculated for NiOMP by using the same force field are substantially lower than the NiOEP values.

Pyrrole swiveling modes are assigned to prominent bands at 612 cm^{-1} in the spectrum of C (γ_{12}, B_{1u}) and at 494 cm^{-1} in the A and B spectra (γ_{22}, E_g). (γ_{22} overlaps with ν_{33} (Table I) but is separated from it by the 11-cm^{-1} downshift upon meso-deuteration (Figure 5)). The pyrrole tilting modes γ_6, γ_{16}, and γ_{23} are assigned to bands at 360, 270, and 254 cm^{-1} in the C spectrum; γ_{23} (E_g) shows up in the A and B spectra (238, 241 cm^{-1}) as well. The γ_6 mode is at an elevated frequency because of interaction with the $\gamma(C_\alpha C_m)$ mode (γ_7), assigned at 284 cm^{-1}. The large d_4 shift, 23 cm^{-1}, reflects this interaction. The γ_6 and γ_7 modes show ^{62}Ni frequency shifts (Figure 4) as expected from the eigenvectors (Figure 12); only A_{2u} modes can involve motions of the Ni atom. The observed shifts, 2.3 and 1 cm^{-1}, are larger than those calculated, 0.9 and 0.3 cm^{-1}, perhaps reflecting the difference between the actual ruffled structure and the flat one used in the calculation. γ_7 (284 cm^{-1}) is mainly $\gamma(C_\alpha C_m)$ in character. The E_g $\gamma(C_\alpha C_m)$ mode, γ_{24}, shows up strongly at 223 cm^{-1} in the triclinic A spectra, while the B_u mode, γ_{13}, which is calculated at 130 cm^{-1}, is not observed.

The lowest frequency band in the C spectrum (Figure 2), a quite prominent one at 127 cm^{-1}, is assigned to the B_{2u} $\gamma(C_\beta C_1)$ mode, γ_{17}, which is calculated and observed to be isotope insensitive. The other $\gamma(C_\beta C_1)$ modes are calculated at low frequencies, 107 cm^{-1} or less, and slightly higher for NiOMP (Table V) due to the lack of coupling with the adjacent $\delta(C_\beta C_1 C_2)$ coordinates in NiOEP. Likewise the A_{2u} γ(NiN) mode, γ_9, in which the Ni atom moves in phase with the tilting of the pyrrole rings (Figure 12) is calculated to have a very low frequency, 32 cm^{-1}.

We note one apparent violation of the selection rule that only E_g modes are activated in the C_{2h} point group of A and B. The spectrum of B contains a band assigned to the A_{1u} mode δ_1 ($\delta(C_\beta C_1 C_2)$) at 437 cm^{-1}, which, however, is missing in the spectrum of A. In the B crystal structure the porphyrin rings show significant stacking interactions[3] with one another.[5] Perhaps the activation of the non-E_g oop mode is also due to this intermolecular effect.

The A_{2u} assignments are supported by the observation of IR counterparts with the same isotope sensitivity at 846, 742, and 360 cm^{-1}.[16,19]

Effect of Ethyl Orientation. As discussed in our previous study,[8b] the low-frequency in-plane modes of NiOEP are influenced by the relative orientations of the ethyl groups. The kinematic coupling between ethyl and porphyrin coordinates is different when the ethyl groups on a given pyrrole ring point in the same or opposite directions. This effect is believed to account for the frequency differences between the A and B triclinic forms, observed especially for the ν_8 and ν_9 modes, which involve coupled Ni–pyrrole breathing and ethyl deformation motions.[8b] The two ethyl groups on each pyrrole ring point in the same direction for A, but for two pyrrole rings in B they point in opposite directions.

It is reasonable to expect similar influences on the out-of-plane modes, to the extent that they are coupled to ethyl motions. As in the case of the in-plane modes,[8b] we investigated the ethyl orientational kinematics, by recalculating the oop modes for a model having the ethyl group pointed alternately up and down around the ring, (structure D in Figure 1 of ref 8b). This model

(17) Czernuszewicz, R. S.; Sheats, J. E.; Spiro, T. G. *Inorg. Chem.* **1987**, *26*, 2063–2067.

(18) (a) Colthup, N. B.; Daley, L. H.; Wiberley, S. E. *Introduction to Infrared Raman Spectrosc.*; Academic Press: New York, 1975; Chapter 8. (b) See, for example: Vavsanyi, G. *Vibrational Spectra of Benzene Derivatives*; Academic Press: New York, 1969; pp 299–350. (c) Sverdlov, L. M.; Kovner, M. A.; Krainov, E. P. In *Vibrational Spectra of Polyatomic Molecules*; John Wiley: New York, 1974; Chapter 6–11.

(19) Kincaid, J. R.; Urban, M. W.; Watanabe, T.; Nakamoto, K. *J. Phys. Chem.* **1983**, *87*, 3096–3101.

Table VI. Classification of NiOEP Out-of-Plane Modes in D_{4h} Symmetry According to the Local-Mode Contributions[a]

local mode	A_{1u}		A_{2u}		B_{1u}		B_{2u}		E_g	
$\gamma(C_mH)$			γ_4	844	γ_{10}	[845][b]			γ_{19}	841[c]
pyr fold$_{asym}$	γ_1	750			γ_{11}	732			γ_{20}	[731]
pyr fold$_{sym}$			γ_5	739[d]			γ_{15}	704	γ_{21}	656[e]
pyr swivel	γ_2	[346]			γ_{12}	612			γ_{22}	494
pyr tilt			γ_6	360			γ_{16}	270	γ_{23}	254[f]
$\gamma(C_\alpha C_m)$			γ_7	284	γ_{13}	[130]			γ_{24}	230[g]
$\gamma(C_\beta C_1)_{sym}$			γ_8	[108]			γ_{17}	127	γ_{25}	[91]
$\gamma(C_\beta C_1)_{asym}$	γ_3	[74]			γ_{14}	[44]			γ_{26}	[63]
pyr transl.							γ_{18}	[30]		
γ(NiN)			γ_9	[32]						
$\delta(C_\beta C_1 C_2)_{sym}$			δ_2	525			δ_4	477[h]	δ_5	552/548
$\delta(C_\beta C_1 C_2)_{asym}$	δ_1	445[i]			δ_3	[392]			δ_6	[382]

[a] See Figure 11 for the description of the local modes and Figure 12 for the normal-mode eigenvectors. All frequencies are from RR spectra of tetragonal (form C) crystals at 12 K, except as indicated in the footnotes. [b] Brackets indicate calculated frequencies, not observed. [c] Seen in triclinic crystal (forms A and B) RR spectra. [d] Observed at 726 cm^{-1} in form B. [e] Observed at 663 cm^{-1} in form A. [f] Observed at 238 and 241 cm^{-1} in forms A and B. [g] Observed at 223 cm^{-1} in form A. [h] Observed at 455 cm^{-1} (strong) in form A and at 463 cm^{-1} (very weak) in form B. [i] Observed at 437 cm^{-1} in form A.

Table VII. Classification of NiTPP Out-of-Plane Modes in D_{4h} Symmetry According to the Local-Mode Contributions[a]

local mode	A_{1u}		A_{2u}		B_{1u}	B_{2u}		E_g	
$\gamma(C_mPh)$			γ_4		γ_{10}			γ_{19}	
pyr fold$_{asym}$	γ_1	621			γ_{11}			γ_{20}	664
pyr fold$_{sym}$			γ_5	575		γ_{15}	605	γ_{21}	547
pyr swivel	γ_2	330			γ_{12}			γ_{22}	456
pyr tilt			γ_6	321		γ_{16}	414	γ_{23}	359
$\gamma(C_\alpha C_m)$			γ_7	251	γ_{13}			γ_{24}	165
$\gamma(C_BH)_{sym}$			γ_8	712		γ_{17}	797	γ_{25}	741
$\gamma(C_\beta H)_{asym}$	γ_3	900			γ_{14}			γ_{26}	915
pyr transl						γ_{18}			
γ(NiN)			γ_9						

[a] All frequencies are froim solid-state RR spectra at room temperature. The order of mode numbering is retained from NiOEP to facilitate comparison.

conforms to D_4 symmetry and allows all the modes to be tracked from the D_{2d} calculation. Kinematically it is the limiting case in which each pyrrole ring has an up and down ethyl group, in contrast to the D_{2d} model having ethyl groups pointed in the same direction on each pyrrole (structure C in Figure 1 of ref 8b).

The results are given in Table V. It can be seen that an orientational kinematic effect is expected and that it is expressed quite selectively, depending on the ethyl mode couplings. Major frequency differences are predicted for the pyrrole folding modes in the 700-cm^{-1} region, γ_1 (B_{1u}), γ_{11} (B_{2u}), and γ_{20} (E_g) each showing 30–40 cm^{-1} up- (γ_1, γ_{11}) or down- (γ_{20}) shifts between the D_{2d} and D_4 calculations. These are precisely the modes that are strongly coupled to the $\delta(C_\beta C_1 C_2)$ coordinates, as revealed by large-frequency upshifts relative to the NiOMP calculation (Table V). The experimental evidence on this point is scanty, since few oop modes are activated in the A and B forms. For δ_4 the frequencies 455 (A) and 463 (B) cm^{-1} are in the predicted order, but the two γ_{23} frequencies 238 (A) and 241 (B) cm^{-1} show almost no difference while a large difference is predicted.

NiTPP and NiP. Table VII classifies the candidate out-of-plane modes of NiTPP that are detected in the 5682-Å excited spectra (Figure 10) and assigned by analogy with the NiOEP modes on the basis of the isotope shifts. We note that in D_{4h} symmetry ^{15}N shifts are excluded for the A_{2u} and B_{2u} modes while methine ^{13}C shifts are excluded for the A_{2u} and B_{1u} modes. Depolarization ratios are not reliable for the NiTPP solid, since the sample was insufficiently absorbing. The assignments are plausible but are less secure than for NiOEP since we have not carried out an oop calculation for NiTPP.

The pyrrole folding modes, all of which are identified by large d_8 downshifts, are at much lower frequencies, 546–665 cm^{-1}, than their NiOEP counterparts, as expected from the relief of the $\delta(C_\beta C_1 C_2)$ coupling. The $\gamma(C_\beta H)$ modes fall into two classes, in-phase (both CH bonds bend in the same direction), at ~700–750 cm^{-1}, and out-of-phase, at 850–900 cm^{-1}. (These bands are seen in the spectra shown in the Figure 11 of ref 8c). Similar phasing effects are seen for benzene and other aromatics;[12,13] the two groups of frequencies bracket the ~850-cm^{-1} frequencies observed for the isolated $\gamma(C_mH)$ bends in NiOEP.

Table VIII. Comparison of A_{2u} Mode Frequencies (cm^{-1}) for Three Ni Porphyrins

local mode[a]	A_{2u}	NiOEP[b]	NiP[c]	NiTPP[b]
$\gamma(C_mX)$	γ_4	844	856	
(pyr fold)$_{sym}$	γ_5	739		575
pyr tilt	γ_6	360	356	321
$\gamma(C_\alpha C_m)$	γ_7	284	282	251
$\gamma(C_\beta Y)_{sym}$	γ_8	[108][d]	698	712
γ(NiN)	γ_9	[32]		

[a] X, Y = H, H for NiP; H, C_2H_5 for NiOEP; and C_6H_5, H for NiTPP. [b] RR frequencies from solid-state spectra at room (NiTPP) and low (tetragonal NiOEP, 12 K) temperatures. [c] IR frequencies (from ref 21). [d] Brackets indicate calculated frequencies; not observed.

The A_{2u} modes are also identifiable in IR spectra,[20] and a 2.5 cm^{-1} ^{62}Ni shift has been reported for the 320-cm^{-1} IR band. This is the basis for assigning the 321-cm^{-1} RR band to the γ_6 pyrrole tilting mode, by analogy with the 360-cm^{-1} band of NiOEP. There seems, however, to be much greater mixing with the A_{1u} $\gamma(C_\alpha C_m)$ mode, γ_7, in the case of NiTPP, since the latter shows a 3-cm^{-1} ^{15}N downshift while γ_6 shifts only 1 cm^{-1}; in contrast the ^{15}N shifts are 5 and 0 cm^{-1} for γ_6 and γ_7 in NiOEP. Another interesting difference is the lack of a candidate γ_{12} pyrrole swiveling mode in NiTPP, seen strongly at 612 cm^{-1} in NiOEP. This NiOEP mode is very sensitive to methine deuteration, and it is unclear what the phenyl substitution does to its frequency or indeed its composition. There is, however, a prominent 330-cm^{-1} band, which, from the lack of ^{15}N or $^{13}C_m$ sensitivity, is assigned to the A_{1u} swiveling mode γ_2, unobserved in NiOEP but calculated at 346 cm^{-1}.

We were unable to find candidate oop bands for Ni porphine (NiP) at any of the available excitation wavelengths.[8b] Infrared spectra,[21] however, implicate bands at 856, 698, 356, and 282 cm^{-1}

(20) Kincaid, J. R.; Nakamoto, K. *J. Inorg. Nucl. Chem.* **1975**, *37*, 85–89.
(21) (a) Ogoshi, H.; Saito, Y.; Nakamoto, K. *J. Chem. Phys.* **1972**, *57*, 4194–4202. (b) Li, X.-Y. Ph.D. Thesis, Princeton University, 1988.

as A_{2u} modes from their d_4 or d_8 shifts. In Table VIII we compare the A_{2u} frequencies for NiOEP, NiP, and NiTPP. NiOEP and NiP have similar frequencies and d_4 shifts for γ_6 and γ_7, suggesting that the apparently altered composition in NiTPP stems from the involvement of the heavy phenyl groups at the C_m bridges.

Implications. Several of the out-of-plane modes deserve comment. The A_{2u} pyrrole tilting mode, γ_6, at 360 cm^{-1}, is in the frequency region of stretching modes for axial ligand bonds, and it may interact with these stretches. A dramatic instance has already been noted for the complex $[(ImH)_2Fe^{III}OEP]^+$ (ImH = imidazole), where coupling of the tilt with the asymmetric $Fe(ImH)_2$ stretch leads to complete mode mixing, with two IR bands, at 385 and 319 cm^{-1}, showing equal isotope shifts upon meso-deuteration as well as ImH perdeuteration.[7] In considering the dynamics of ligand dissociation in heme proteins, it is reasonable to expect that the γ_6 pyrrole tilting mode, as well as the lower frequency A_{2u} modes γ_8 and γ_9, in which the metal atom is strongly displaced, will play a role.

Another mode of interest is the B_{1u} pyrrole swiveling mode γ_{12}, at 612 cm^{-1}. This mode resembles the ruffling distortion seen in the tetragonal crystals.[3] As discussed in the following article,[8a] this mode is believed to soften in solution, leading to a distribution of ruffled structures, due to the competition between porphyrin flattening and the NiN bond shortening which ruffling permits.

We also call attention to the B_{2u} pyrrole translation mode, γ_{17} at 127 cm^{-1}. This mode involves translational displacement of the pyrrole rings up to and down from the porphyrin plane. A distortion of this form is seen in crystal structures of several porphyrin radical cations,[22] and we argue elsewhere[23] that this distortion may be an intrinsic electronic effect associated with pseudo-Jahn–Teller mixing of the ground state with a low-lying excited state.

(22) Scheidt, W. R.; Lee, V. J. *Struct. Bonding* **1987**, *64*, 1–70.
(23) Czernuszewicz, R. S.; Macor, K.; Li, X-Y.; Kincaid, J. A.; Spiro, T. G. *J. Am. Chem. Soc.* **1989**, *111*, 3860–3869.

The $\gamma(C_\beta C_1 C_2)$ ethyl modes are calculated to have a major perturbing effect on the out-of-plane frequencies, especially in regard to the pyrrole folding modes (Table V). This fact is important when OEP complexes are used as models for heme proteins, most of which contain protoporphyrin IX (PP). The substituents of PP are four methyl, two vinyl, and two propionate groups. The propionate alkyl chains should resemble ethyl substituents with regard to the kinematic coupling, but the methyl and vinyl groups will not. Thus a larger frequency spread of the out-of-plane modes can be expected for PP than for OEP.

Conclusion

From high-quality low-temperature RR spectra of crystalline NiOEP in its three polymorphs it has been possible to assign a majority of the out-of-plane modes via polarization and isotope shift measurements. A force field has been developed that gives a satisfactory account of these modes in terms of the isotope shift pattern. Some frequencies deviate appreciably from observed values, perhaps reflecting the effect of the porphyrin ruffling in structure C, which provides most of the data. Tentative assignments are also given for NiTPP. Of particular interest are the modes associated with cooperative motions of the pyrrole rings, tilting, swiveling, and translation, which are connected with static and dynamic structural distortions of metalloporphyrins. The ethyl bending modes of NiOEP have a major perturbing effect on the out-of-plane mode frequencies, which will have to be taken into account in extending the analysis to heme proteins.

Acknowledgment. This work was supported by NIH Grants GM 33576 (T.G.S.) and DK 35153 (J.R.K.).

Registry No. NiOEP, 24803-99-4; D_2, 7782-39-0; ^{15}N, 14390-96-6.

Supplementary Material Available: Figures showing atom numbering of NiOEP and NiOMP and definition of valence force field and interaction terms for NiOEP and tables of structural parameters, Cartesian coordinates, and unnormalized U matrix for NiOEP (14 pages). Ordering information is given on any current masthead page.